Aerodynamic Flow Effects on Aircraft Carrier Takeoff Performance

R. Bardera-Mora[1], A. Garcia-Magariño[2]

Instituto Nacional de Técnica Aeroespacial (INTA), Torrejón de Ardoz, Madrid, 28850, Spain,

A. Rodríguez-Sevillano[3] and M. A. Barcala-Montejano[4]

ETSI Aeronáutica y del Espacio, Universidad Politécnica de Madrid (UPM), Madrid, 28040, Spain

The aircraft take-off manoeuvre for on-board operations is the most critical aspect of maritime performance. In the last decades, several improvements have been made in order to reduce the number of accidents. One of them is the Ski-Jump Ramp, a modern take-off system that allows the manoeuvre to be performed more safely and using less runway distance. Thus, a new in-depth aerodynamic study of the ramp is required. A wind tunnel test campaign was developed in order to study the disturbances caused by the ski-jump ramp over the flight deck and the influence on an aircraft carrier performance. Smoke visualizations over the ramp revealed a detached unsteady recirculation bubble at the ramp and a turbulent flow over the flight deck. Velocity measurements were carried out by means of Particle Image Velocimetry. The influence of these disturbances was evaluated for the take-off performance of the AV-8B Harrier II. The results proved the importance of taking into account these disturbance effects and provided a detailed characterization of the flow over the carrier-deck, resulting in establishment of a useful background for future studies on aircraft-ship interference.

1 PhD Aerospace Engineer, Experimental Aerodynamic, barderar@inta.es,
2 PhD Aerospace Engineer, Experimental Aerodynamic, garciamga@inta.es,
3 Professor , Flight Mechanics, angel.rodriguez.sevillano@upm.es,
4 Professor, Aerodynamics, miguel.barcala@upm.es.

Published by the American Institute of Aeronautics and Astronautics, Inc., with permission. Complete Citation: Bardera-Mora, R., Garcia-Magariño, A., Rodríguez-Sevillano, A., & Barcala-Montejano, M. A. (2019). Aerodynamic flow effects on aircraft carrier takeoff performance. Journal of Aircraft, 56(3), 1005-1013. https://doi.org/10.2514/1.C035188

Nomenclature

α	=	angle of attack
C_D	=	drag coefficient
C_{D0}, k	=	drag polar coefficients
C_L	=	lift coefficient
C_{L0}, $C_{L\alpha}$	=	lift coefficient parameters
D	=	aerodynamic drag force
ε	=	thrust angle
g	=	gravity acceleration
h	=	height of the ski-jump ramp from the deck of the model
H	=	height of the model
L	=	aerodynamic lift force
L_r	=	ski-jump ramp length
L_{T0}	=	take-off runway horizontal distance
μ	=	rolling friction coefficient
n	=	load factor
Π_1 Π_2, Π_3	=	non-dimensional parameter of the equation models
R	=	radius of curvature of the ramp
R_1, R_2	=	reaction forces
ρ	=	air density
S	=	surface area
s	=	spatial position along the aircraft path in the curved part
σ_{tot}	=	total standard deviation of the velocity magnitude
t	=	time
T	=	thrust force

Published by the American Institute of Aeronautics and Astronautics, Inc., with permission. Complete Citation: Bardera-Mora, R., Garcia-Magariño, A., Rodríguez-Sevillano, A., & Barcala-Montejano, M. A. (2019). Aerodynamic flow effects on aircraft carrier takeoff performance. Journal of Aircraft, 56(3), 1005-1013. https://doi.org/10.2514/1.C035188

TI	=	turbulence intensity
θ	=	local angle at a generic point of the ramp
$\overrightarrow{u_{\parallel}}$	=	unit vector parallel to the deck in the stream wise direction
$\overrightarrow{u_{\perp}}$	=	unit vector perpendicular to the deck
U_{∞}	=	undisturbed wind velocity respect to the carrier
$\vec{V}_a$	=	aerodynamic velocity
$\vec{V}_f$	=	aircraft velocity respect to the carrier
$\vec{V}_S$	=	aircraft carrier velocity
$\vec{V}_W$	=	atmospheric headwind velocity
$\vec{V}_{WOD}$	=	relative wind velocity over the deck
W	=	weight force
x	=	horizontal coordinate
x_1	=	horizontal coordinate in PIV axis
z_1	=	vertical coordinate in PIV axis
$\wedge$	=	indicates that the variable is non-dimensional

I. Introduction

The importance of the aircraft carrier has grown rapidly in the latest decades. The modern aircraft carrier enables to operate aircraft close to the conflict zone without owning infrastructure in those regions. Very recently, two studies have been conducted related to the use of carrier-based unmanned aerial vehicles onboard [1-2]. However, the naval environment is not the most suitable for operating aircraft. The incident atmospheric wind and the inherent turbulence of the flow make the aerodynamic environment in the vicinity of a ship highly complex [3].

The most critical step for aircraft in overseas operations is the take-off manoeuvre. The main objective is to perform the manoeuvre in the shortest distance possible, due to the shorter runway distance available on the ship compared to the traditional land-based operations. There are mainly two ways to shorten this distance: the catapult assisted take-off and the ski-jump ramp take-off. A presentation of the electromagnetic catapulting aircraft launch system-EMALS

Published by the American Institute of Aeronautics and Astronautics, Inc., with permission. Complete Citation: Bardera-Mora, R., Garcia-Magariño, A., Rodríguez-Sevillano, A., & Barcala-Montejano, M. A. (2019). Aerodynamic flow effects on aircraft carrier takeoff performance. Journal of Aircraft, 56(3), 1005-1013. https://doi.org/10.2514/1.C035188

and a simulation of the carried-based aircraft catapult launch can be found in the articles of Doyle et al. [4] and Weijun et al[5], respectively. Also, another very comprehensive study with the catapult launch is the one of Qian et al. [6], which is based on a carrier-aircraft multi-agent system simulation model.

The ski-jump ramp, which enables the aircraft to perform the manoeuvre using less runway distance and allows safer take-off operations, as shown by Clark and Walters[7], has the advantage of simplicity as compared to catapult system; however special attention should be paid to the aerodynamic effects of the ski-jump ramp. In a previous study by some of the authors[6], the flow field in the region of the ski-jump was investigated showing the existence of a recirculation bubble formed downstream of the ramp. In this study[8], the main objective was to assess the use of passive control actuators to reduce the recirculation bubble, and only the region at the beginning of the sky-jump, where the recirculation bubble was found, was investigated. Others previous studies concerning the ski-jump ramp, that include those of Fozard[9], Fry et al.[10], Wei-Wei and Xiang-Ju[11], Yagang et al.[12] and Liu et al.[1] did not even considered this recirculation bubble. The study of Fozard is presented in a very earlier paper[9] that contains the history and explains the appearance of the ski-jump as a tactic to increase the weight of the aircraft while taking off from an aircraft carrier (due to the lower power required to take –off). In the paper, the ski-jump principles and the operational implication were posed. Fry et al.[10] conducted an optimization of the ski-jump ramp profile for the F-35B Lightning. Both Wei-Wei and Xiang-Ju [11]and Yagang et al.[12] modelled the problem as a whole, considering the carrier, the landing gear and the aircraft as integrated parts. Wei-Wei and Xiang-Ju [11] developed the equations for a based on tensor model while Yagang et al.[12] made use of a multi-body dynamic system simulation, that also considered the wind field induced by the aircraft carrier, the command decision on deck and the control policy of the model.

Aerodynamic effects of the ski-jump ramp[6] propagate downstream along the flight deck and through the rest of the ship. The ski-jump presence generates a thicker boundary layer on the runway with a recirculated bubble and a turbulent shear layer that transport turbulent studies downstream. The take-off manoeuvres are conducted along the flight deck. Therefore, full understanding of the flow and its influence in the take-off manoeuvre is required. Instead of studying only the beginning of the sky-jump, the aim of this study is to extend the previous study[8]and to characterize the flow over all the flight deck of an aircraft carrier in order to get a more precise insight about the turbulent flow developed over the ski-jump ramp that propagates downstream and the adverse effects induced on the aircraft during take-off operations. First of all, the flight mechanics equations of an aircraft along the take-off runway are inferred. Then, a visualization of the flow along the flight deck is presented. Following, the flow field is quantified by means

Published by the American Institute of Aeronautics and Astronautics, Inc., with permission. Complete Citation: Bardera-Mora, R., Garcia-Magariño, A., Rodríguez-Sevillano, A., & Barcala-Montejano, M. A. (2019). Aerodynamic flow effects on aircraft carrier takeoff performance. Journal of Aircraft, 56(3), 1005-1013. https://doi.org/10.2514/1.C035188

of new Particle Image Velocimetry (PIV) measurements along all the flight deck, leading to analytical functions for the wind velocity along the flight path of the aircraft. Next, a study of the influence of the ski-jump in the take-off of the aircraft is performed by studying the take-off performance of the AV-8B Harrier II and finally conclusions are given.

II. Take-Off Flight Mechanics

The take-off procedure is studied by applying the classical Flight Mechanics equations to the aircraft centre of mass expressed in axes parallel and normal to the deck and neglecting ground effects [13-15]. The aircraft is assumed to follow the take-off run path until the end of the run and the momentum equations are considered. Figure 1 shows the

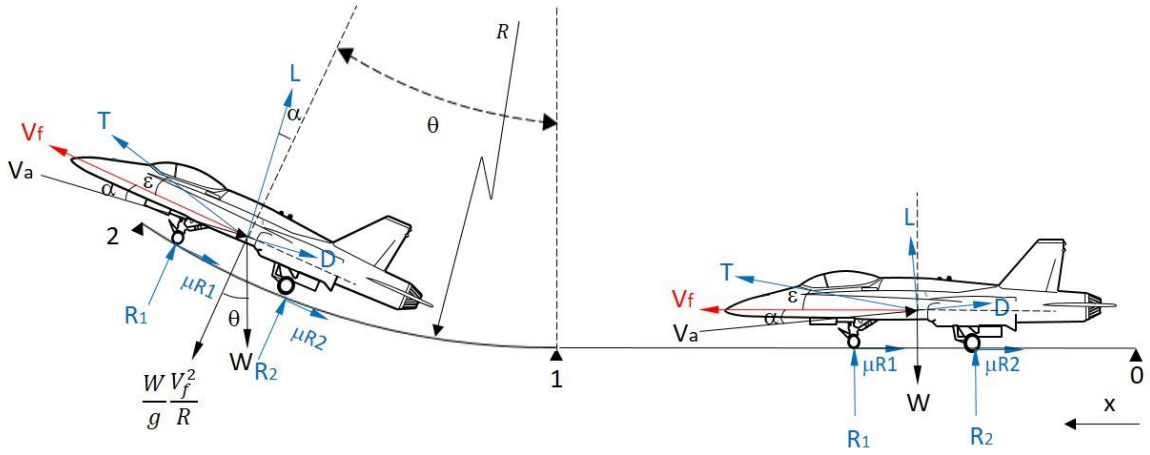

$$\frac{W}{g}\frac{dV_f}{dt} = T\cos\varepsilon - D\cos\alpha + L\sin\alpha - \mu(R_1 + R_2) - W\sin\theta$$

$$\frac{W}{g}\frac{V_f^2}{R} = T\sin\varepsilon + L\cos\alpha + D\sin\alpha + (R_1 + R_2) - W\cos\theta$$

$$\frac{W}{g}\frac{dV_f}{dt} = T\cos\varepsilon - D\cos\alpha + L\sin\alpha - \mu(R_1 + R_2)$$

$$0 = T\sin\varepsilon + L\cos\alpha + D\sin\alpha + (R_1 + R_2) - W$$

Figure 1. Aircraft flight mechanics in take-off manoeuvre.

forces acting on the aircraft during the take-off run which are the thrust T, the aerodynamic lift L, the aerodynamic drag D, the weight W, the reaction forces R_1 and R_2 and the friction forces $\mu R_1$and μR_2.

The case of study considered here is the case in which the atmospheric headwind velocity $\vec{V}_W$ that is blowing over the ship is aligned with the aircraft carrier motion $\vec{V}_S$ and the ship is moving in rectilinear cruise inducing a relative wind velocity over the deck (respect to the carrier) denoted as $\vec{V}_{WOD}$. The problem is divided into the horizontal run part (denoted as 0-1) and the curved ski ramp part (denoted as 1-2). The generic equations for each part are written in

Published by the American Institute of Aeronautics and Astronautics, Inc., with permission. Complete Citation: Bardera-Mora, R., Garcia-Magariño, A., Rodríguez-Sevillano, A., & Barcala-Montejano, M. A. (2019). Aerodynamic flow effects on aircraft carrier takeoff performance. Journal of Aircraft, 56(3), 1005-1013. https://doi.org/10.2514/1.C035188

Fig. 1 below the corresponding part. In Fig. 1 and in the following equations g stands for the gravity, t for time, μ for the rolling friction coefficient, ε for the thrust angle, Vf for the aircraft velocity respect to the carrier, Va for the aerodynamic velocity, R for the radius of curvature of the ramp, θ for the local angle at a generic point of the ramp and α for the angle of attack. However, if it is assumed that the thrust is aligned to the surface and therefore the angle of thrust ε is negligible, and the angle of attack is small ($\cos(\alpha) \cong 1$, $\sin(\alpha) \cong \alpha$), then according to the book of Anderson[16], in pages 356 and 359, equations in the horizontal run part (0-1) can be combined to give,

$$\frac{W}{g}\frac{dV_f}{dt} = T - \mu W - D + L(\mu + \alpha) \tag{1}$$

The aerodynamic drag and lift force can be calculated as the product of the dynamic pressure and their corresponding coefficient (Anderson[16], page 205):

$$L = \frac{1}{2}\rho S V_a^2 C_L \tag{2}$$

$$D = \frac{1}{2}\rho S V_a^2 C_D \tag{3}$$

In the Eqs. (2) and (3), ρ is the air density, Va is the modulus of the aerodynamic velocity, S is the wing surface and C_L and C_D are the lift and drag coefficients, respectively. The lift coefficient is a function that depends on the angle of attack α as follows:

$$C_L = C_{L0} + C_{L\alpha}\alpha \tag{4}$$

where C_{L0} and $C_{L\alpha}$ are constants. The drag coefficient can be expressed as a function of the lift coefficient, using the aircraft aerodynamic polar (Anderson[16], page 130):

$$C_D = C_{D0} + k\, C_L^2 \tag{5}$$

Published by the American Institute of Aeronautics and Astronautics, Inc., with permission. Complete Citation: Bardera-Mora, R., Garcia-Magariño, A., Rodríguez-Sevillano, A., & Barcala-Montejano, M. A. (2019). Aerodynamic flow effects on aircraft carrier takeoff performance. Journal of Aircraft, 56(3), 1005-1013. https://doi.org/10.2514/1.C035188

The aerodynamic velocity $\vec{V}_a$ is the relative velocity between the air velocity over the deck $\vec{V}_{WOD}$ and the aircraft velocity respect to the carrier $\vec{V}_f$,

$$\vec{V}_a = \vec{V}_{WOD} - \vec{V}_f \tag{6}$$

The wind velocity over deck $\vec{V}_{WOD}$ can be decomposed in a component parallel to the deck (denoted as $V_{wod_\parallel}$), which in general opposes the aircraft movement and another component normal to the deck (denoted as $V_{wod_\perp}$).

$$\vec{V}_{WOD} = -V_{WOD_\parallel}\overrightarrow{u_\parallel} + V_{WOD_\perp}\overrightarrow{u_\perp} \tag{7}$$

In Eq. (7), $\overrightarrow{u_\parallel}$ is a unit vector parallel to the deck in the direction of the aircraft movement and $\overrightarrow{u_\perp}$ is the unit vector normal to the deck. The aircraft velocity has only one component parallel to the deck $\vec{V}_f = V_f\vec{u}_\parallel$. The modulus of the aerodynamic velocity V_a can be expressed as:

$$V_a{}^2 = (V_f + V_{WOD_\parallel})^2 + (V_{WOD_\perp})^2 \tag{8}$$

The angle of attack is considered to be the angle between the aerodynamic velocity and the aircraft velocity, which is obtained by geometrical considerations:

$$\alpha = \tan^{-1}\left(\frac{V_{WOD_\perp}}{V_f + V_{WOD_\parallel}}\right) \tag{9}$$

By introducing the previous expressions into Eq. (1), and changing the independent variable by using $V_f = \frac{dx}{dt}$, (Note that $\frac{dV_f}{dt} = \frac{dV_f}{dx}\cdot\frac{dx}{dt} = \frac{dV_f}{dx}\cdot V_f$), a final expression is obtained for the horizontal run part (0-1), as in the book of Miele[14] in page 275:

Published by the American Institute of Aeronautics and Astronautics, Inc., with permission. Complete Citation: Bardera-Mora, R., Garcia-Magariño, A., Rodríguez-Sevillano, A., & Barcala-Montejano, M. A. (2019). Aerodynamic flow effects on aircraft carrier takeoff performance. Journal of Aircraft, 56(3), 1005-1013. https://doi.org/10.2514/1.C035188

$$V_f \frac{dV_f}{dx} = \frac{g}{W}\left[(T - \mu W) - \frac{1}{2}\rho S[C_D - (\mu + \alpha)C_L]V_a^2\right] \quad (10)$$

where x is the horizontal coordinate defined in Fig. 1, and C_L , C_D , V_a and α are defined in Eqs. (4), (5), (8) and (9) respectively. If the components $V_{WOD_\parallel}$ and $V_{WOD_\perp}$ are known functions of the variable x, then the Eq. (10) can be solved to obtain the aircraft velocity V_f against the variable x.

Equations for the ski-jump ramp are depicted in Fig. 1 on the left part. Assuming that the angle of thrust ε is considered negligible and the angle of attack is small ($\cos(\alpha) \cong 1$, $\sin(\alpha) \cong \alpha$), following a similar scheme as in Barlow et al [15] , equations corresponding to this part (1-2) can be combined to become,

$$\frac{W}{g}\frac{dV_f}{dt} = \left[T - W(\mu\cos\theta + \sin\theta) - D(1 - \mu\alpha) + L(\alpha + \mu) - \frac{\mu W {V_f}^2}{gR}\right] \quad (11)$$

If s is defined as the spatial position along the aircraft path in the curved part, the aircraft velocity respect to the carrier can be defined as $V_f = ds/dt$. This coordinate s depends on the local angle θ as $ds = Rd\theta$. By introducing this in a change in the independent variable $dt = \frac{ds}{V_f} = \frac{Rd\theta}{V_f}$, (Note that $\frac{dV_f}{dt} = \frac{dV_f}{ds}\cdot\frac{ds}{d\theta}\cdot\frac{d\theta}{dt} = \frac{dV_f}{dx}\cdot\frac{V_f}{R}$) and also Eqs. (2), (3) and (9), the previous Eq. (11) can be expressed as follows:

$$V_f \frac{dV_f}{d\theta} = \frac{R\cdot g}{W}\left(T - W(\mu\cos\theta + \sin\theta) - \frac{1}{2}\rho S[C_D(1 - \mu\alpha) - (\mu + \alpha)C_L]V_a^2 - \frac{\mu W {V_f}^2}{gR}\right) \quad (12)$$

where θ is the local angle defined in Fig. 1, and C_L , C_D , V_a and α are defined in Eqs. (4), (5), (8) and (9) respectively. If the components $V_{WOD_\parallel}$ and $V_{WOD_\perp}$ are known functions of the variable θ, then the Eq. (12) can be solved to obtain the aircraft velocity V_f against the variable θ. The variable θ and the variable x are related by geometrical considerations using the following expression:

$$x = x_1 + R\sin(\theta) \quad (13)$$

Published by the American Institute of Aeronautics and Astronautics, Inc., with permission. Complete Citation: Bardera-Mora, R., Garcia-Magariño, A., Rodríguez-Sevillano, A., & Barcala-Montejano, M. A. (2019). Aerodynamic flow effects on aircraft carrier takeoff performance. Journal of Aircraft, 56(3), 1005-1013. https://doi.org/10.2514/1.C035188

where x_1 corresponds to the value of the horizontal coordinate x at the location where the ramp starts. Now, it is convenient to rewrite the Eqs. (8), (9), (10) and (12) in dimensionless form. To this end, the following dimensionless variables and parameters are defined:

$$\hat{x} = \frac{x}{L_{T0}} \ , \hat{V}_f = \frac{V_f}{U_\infty} \ , \hat{V}_{WOD_\parallel} = \frac{V_{WOD_\parallel}}{U_\infty} \ , \hat{V}_{WOD_\perp} = \frac{V_{WOD_\perp}}{U_\infty} \ , \hat{V}_a = \frac{V_a}{U_\infty}, \qquad \hat{T} = \frac{T}{W} \tag{14}$$

where L_{T0} is the take-off runway horizontal distance and U_∞ is the undisturbed wind velocity respect to the carrier $U_\infty = V_W + V_S$. Using these dimensionless variables, the Eqs. (8), (9), (10) and (12) are written as:

$$\frac{d\hat{V}_f}{d\hat{x}} = \frac{\Pi_1}{\hat{V}_f}\left[\hat{T} - \mu - \Pi_2\left[C_D - (\mu + \alpha)C_L\right]\hat{V}_a^2\right] \tag{15}$$

$$\frac{d\hat{V}_f}{d\theta} = \frac{\Pi_3}{\hat{V}_f}\left(\hat{T} - \mu\cos\theta + \sin\theta - \Pi_2\left[C_D(1 - \mu\alpha) - (\mu + \alpha)C_L\right]\hat{V}_a^2\right) - \mu\hat{V}_f \tag{16}$$

$$\hat{V}_a^2 = \left[\left(\hat{V}_f + \hat{V}_{WOD_\parallel}\right)^2 + \left(\hat{V}_{WOD_\perp}\right)^2\right] \tag{17}$$

$$\alpha = \tan^{-1}\left(\frac{\hat{V}_{WOD_\perp}}{\hat{V}_f + \hat{V}_{WOD_\parallel}}\right) \tag{18}$$

where:

$$\Pi_1 = g \cdot \frac{L_{T0}}{U_\infty^2} \tag{19}$$

$$\Pi_2 = \frac{\frac{1}{2}\rho U_\infty^2 S}{W} \tag{20}$$

$$\Pi_3 = g \cdot \frac{R}{U_\infty^2} \tag{21}$$

Published by the American Institute of Aeronautics and Astronautics, Inc., with permission. Complete Citation: Bardera-Mora, R., Garcia-Magariño, A., Rodríguez-Sevillano, A., & Barcala-Montejano, M. A. (2019). Aerodynamic flow effects on aircraft carrier takeoff performance. Journal of Aircraft, 56(3), 1005-1013. https://doi.org/10.2514/1.C035188

III. Aerodynamic Flow over the Flight Deck

In the previous section, the equations for the movement of the aircraft along the take-off run-way were posed. The components of the wind over deck $\hat{V}_{WOD_{\parallel}}$ and $\hat{V}_{WOD_{\perp}}$ as functions of either the dimensionless horizontal coordinate $\hat{x}$ or the local angle θ are necessary to integrate the equations. The aim of this section is to provide a detailed

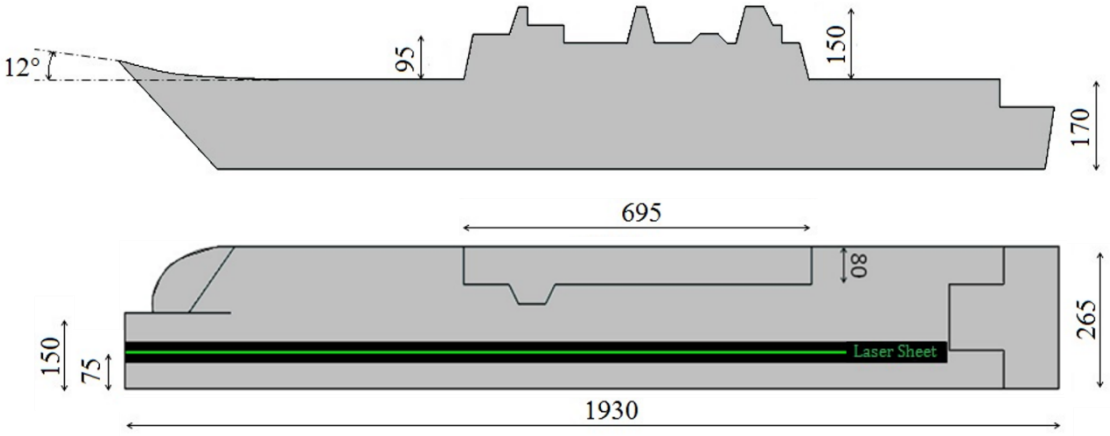

Figure 2.Top and side view of the ship model (dimensions in mm).

characterization of the flow field over the deck and to obtain these functions for the wind over deck components. Wind tunnel experiments were carried out to this end.

A. Experimental Setup

The experiments were conducted in a low speed wind tunnel at INTA (Spain). The wind tunnel is a closed-circuit wind tunnel type with an open test section of 2×3 m^2 and a maximum airspeed of 60 m/s with a turbulence level lower than 0.5%. The test section has a platform, which simulates the ocean surface and hides the part of the hull underwater. Streamlined leading and trailing edges were installed to minimize the interference of the platform in the flow field.

The study was developed for a scaled 1:120 aircraft carrier model with curved ski-jump ramp system (see Fig. 2 and Fig. 3). The model has a length of 1930 mm and a beam of 265 mm.

The height of the ski-jump ramp defined as h is 40 mm and the length L_r is 377 mm. The ski-jump is shaped as a circular arc defined by its radius of curvature R = 1375 mm and the tangential deck angle above the horizon θ_2 = 12° (see Fig. 3). The island superstructure includes the bridge, stacks, radomes and antennas.

Published by the American Institute of Aeronautics and Astronautics, Inc., with permission. Complete Citation: Bardera-Mora, R., Garcia-Magariño, A., Rodríguez-Sevillano, A., & Barcala-Montejano, M. A. (2019). Aerodynamic flow effects on aircraft carrier takeoff performance. Journal of Aircraft, 56(3), 1005-1013. https://doi.org/10.2514/1.C035188

In this experiment, the freestream velocity was $U_\infty = 10$ m/s and the width of the ship is usually selected as the reference length, thus the Reynolds number based on the ramp width for the model was $Re = 1.2\times10^5$ which is above

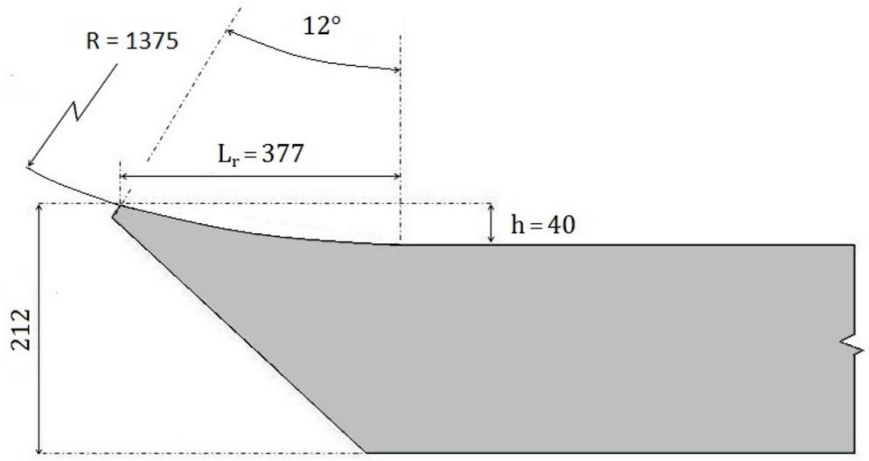

Figure 3. View of the take-off ramp of the model (dimensions in mm).

the critical Reynolds number (1.1×10^4) required for this kind of problem as stated by Healey[17], ensuring the physical similarity with the full-scale problem.

Flow Visualization

In order to understand the aerodynamic phenomena taking place in the take-off ramp, flow visualization with smoke particles was performed in the plane of the path of the aircraft (the same plane as the laser sheet used in PIV experiments). The experiments were carried out with a freestream velocity of 10 m/s. An injector connected to a Rosco Fog Machine model 1900 was placed upstream of the take-off ramp. Figure 4 shows the results of the experiment over the ski-jump ramp, for two different camera exposition times: 1/80 s for the image above and 1/800 s for the image below.

When the smoke is transported by a laminar flow, streamlines can be observed, but if the visualization smoke is transported by turbulent flow structures, streamlines are mixed and consequently individual streamlines cannot be discerned as showed in the image above in Fig. 4. Therefore, the visualization shows the turbulent nature of the flow over the ski-jump ramp. The airflow over the ramp is characterised by a detached recirculation bubble at the bow of

Published by the American Institute of Aeronautics and Astronautics, Inc., with permission. Complete Citation: Bardera-Mora, R., Garcia-Magariño, A., Rodríguez-Sevillano, A., & Barcala-Montejano, M. A. (2019). Aerodynamic flow effects on aircraft carrier takeoff performance. Journal of Aircraft, 56(3), 1005-1013. https://doi.org/10.2514/1.C035188

the ship, which probably introduces high levels of turbulence into the flow field, as shown in the image below in Fig.4. Additionally, the reattachment point can be observed in the image below in Fig 4, in which the camera exposure time was reduced to 1/800 s.

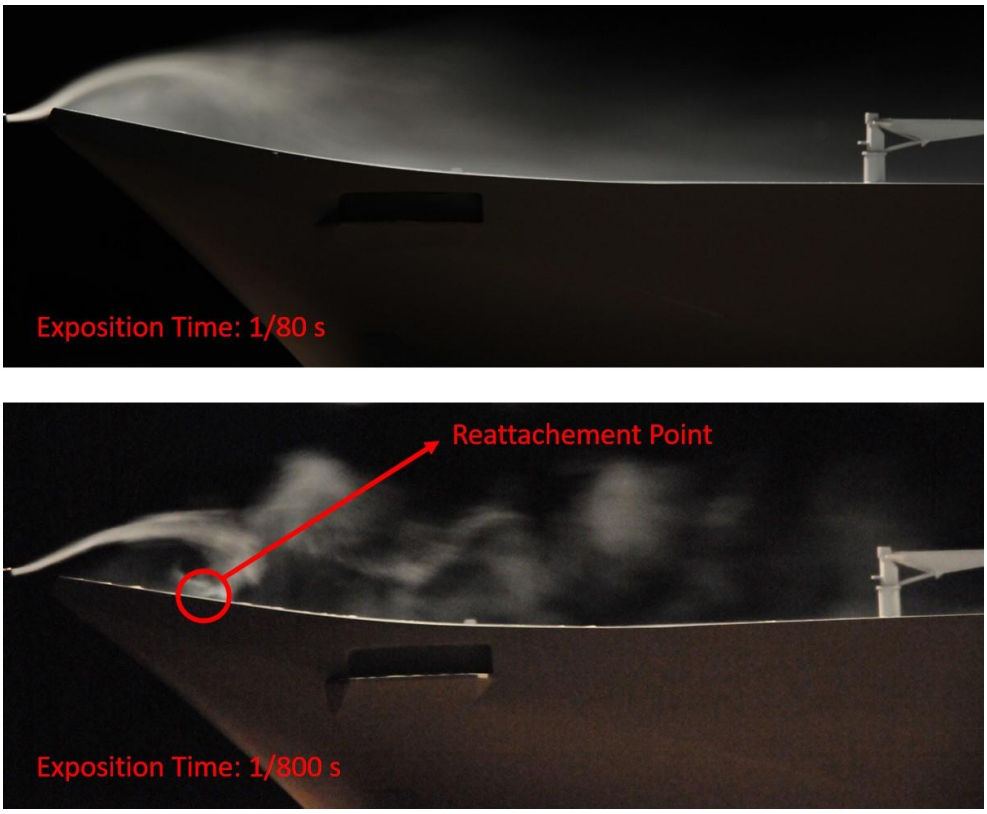

Figure 4. Detailed view of smoke visualization over take-off ramp.

Particle Image Velocimetry

The flow field was investigated by means of Particle Image Velocimetry (PIV). This is a quantitative flow visualization technique used to obtain instantaneous flow field velocity, based on the velocity measurements of the tracer particles transported by the flow[18-21]. Olive oil particles with 1 μm in diameter were generated by a Laskin nozzle to seed the air flow[22-23]. Two Nd:YAG (Neodymium: Yttrium Aluminium Garnet) lasers were used to illuminate the flow. Each laser delivers a maximum energy output of 190 mJ per pulse and a pulse separation of 50μs was used. The pulse width was 9 ns to obtain frozen particles images.

Published by the American Institute of Aeronautics and Astronautics, Inc., with permission. Complete Citation: Bardera-Mora, R., Garcia-Magariño, A., Rodríguez-Sevillano, A., & Barcala-Montejano, M. A. (2019). Aerodynamic flow effects on aircraft carrier takeoff performance. Journal of Aircraft, 56(3), 1005-1013. https://doi.org/10.2514/1.C035188

Images were captured with a “PowerView 4M Plus” high resolution CCD (Charged Coupled Device) camera, in addition with an ED AF Nikkor 80-200mm camera lens. A synchronizer controlled the time interval between laser pulses and the camera captions. The camera field of view (FOV) was 255×255mm^2.

PIV images were divided in regions of 32×32 pixels known as interrogation windows, with a 50% window overlapping according to the Nyquist sampling criteria[24]. The correlation peak was located with subpixel accuracy by fitting a Gaussian curve. Finally, post-processing analysis by a local mean filter size of 3×3 was computed filling holes in the vector maps caused by spurious vectors.

The resulting images were obtained by calculating the averaged field over 200 instantaneous maps. Once obtained, the mean flow velocity field can be processed to obtain non dimensional velocity maps or turbulence distribution, among others. To evaluate the uncertainty, the total standard deviation was calculated for a subset of 100 instantaneous maps and compared to the one obtained over 200 instantaneous maps. Figure 5 shows the total standard deviation inside the recirculated bubble against the horizontal coordinate of the PIV axis, being the total standard deviation calculated using the standard deviation of the components of the velocity as $\sigma_{\text{tot}} = \sqrt{\sigma_u^2 + \sigma_v^2}$. It can be observed that the difference remains below 2.5 m/s, which will lead to a turbulence intensity uncertainty on the order of 2.5%.

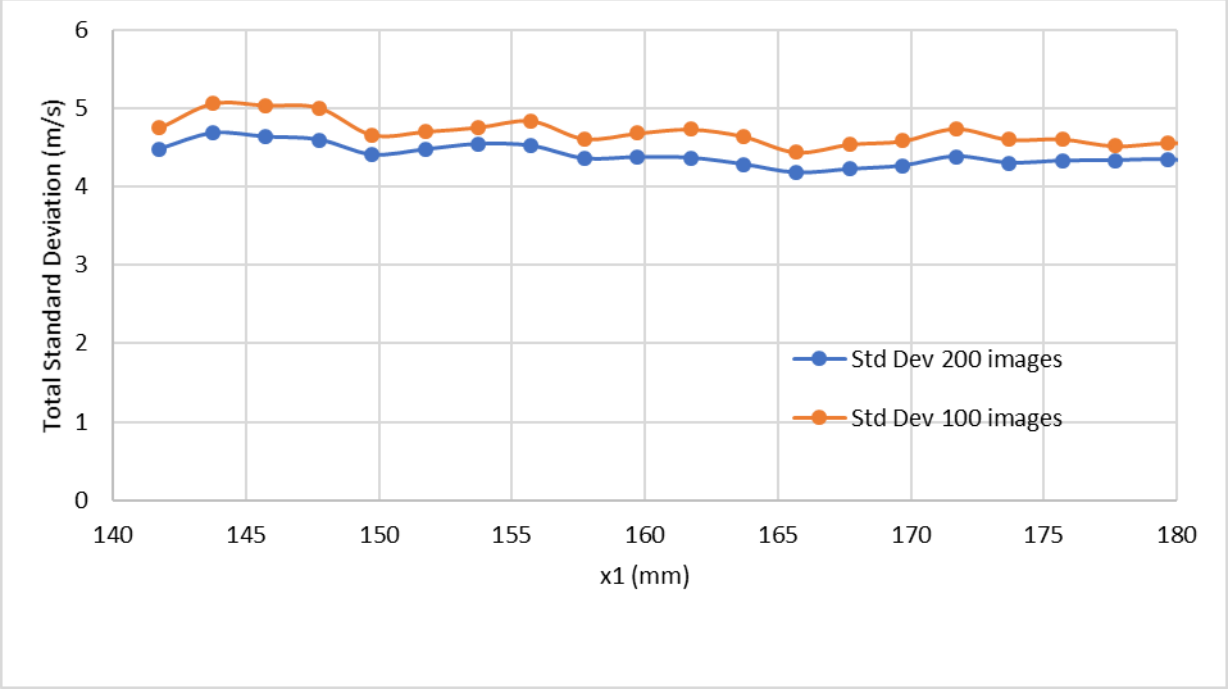

Figure 5. Total Standard Deviation over 100 images and 200 images in frame 1 at y_1 = -121.785 mm.

Published by the American Institute of Aeronautics and Astronautics, Inc., with permission. Complete Citation: Bardera-Mora, R., Garcia-Magariño, A., Rodríguez-Sevillano, A., & Barcala-Montejano, M. A. (2019). Aerodynamic flow effects on aircraft carrier takeoff performance. Journal of Aircraft, 56(3), 1005-1013. https://doi.org/10.2514/1.C035188

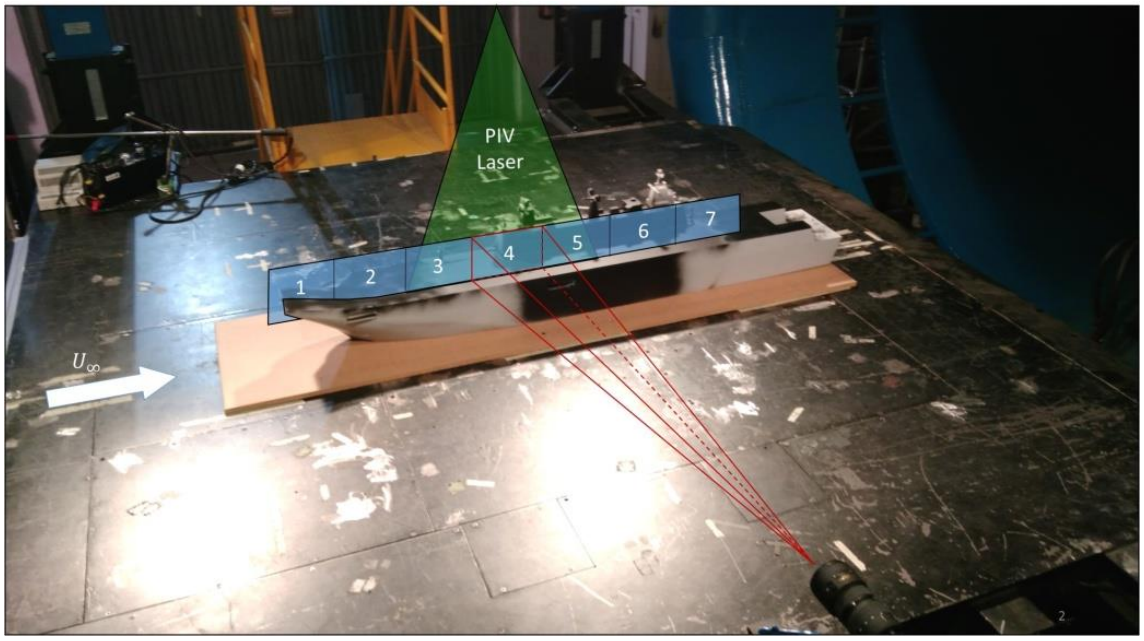

Figure 6. Particle image velocimetry field of view.

As Fig. 6 shows, the take-off runway was divided in 7 frames with a width of 255 mm. This was decided because it was not possible to obtain the required velocity accuracy in a single picture. One by one, the seven frames were analyzed, thereby obtaining velocity and turbulence fields. Then, based on the data from each of the frames, a single data file was built in order to gather all the information in one picture (a coordinate origin change was needed). To join the 7 frames in a single one, an interpolating surface was calculated with the data from each of the frames.

The tests were carried out with the wind tunnel flow aligned to the longitudinal-axis of the ship (zero yaw angle) and illuminating the vertical symmetry plane of the flight deck runway.

B. PIV results

Results obtained from PIV experiments are presented by means of classical maps. Figure 7 shows the non-dimensional flow field velocity along the complete take-off runway. The sharp-edged ramp produces a strong perturbation into the airflow. It generates a recirculation bubble with lower velocity than freestream whereas the flow outer the bubble is accelerated giving an augmentation of the velocity up to 30%.

Published by the American Institute of Aeronautics and Astronautics, Inc., with permission. Complete Citation: Bardera-Mora, R., Garcia-Magariño, A., Rodríguez-Sevillano, A., & Barcala-Montejano, M. A. (2019). Aerodynamic flow effects on aircraft carrier takeoff performance. Journal of Aircraft, 56(3), 1005-1013. https://doi.org/10.2514/1.C035188

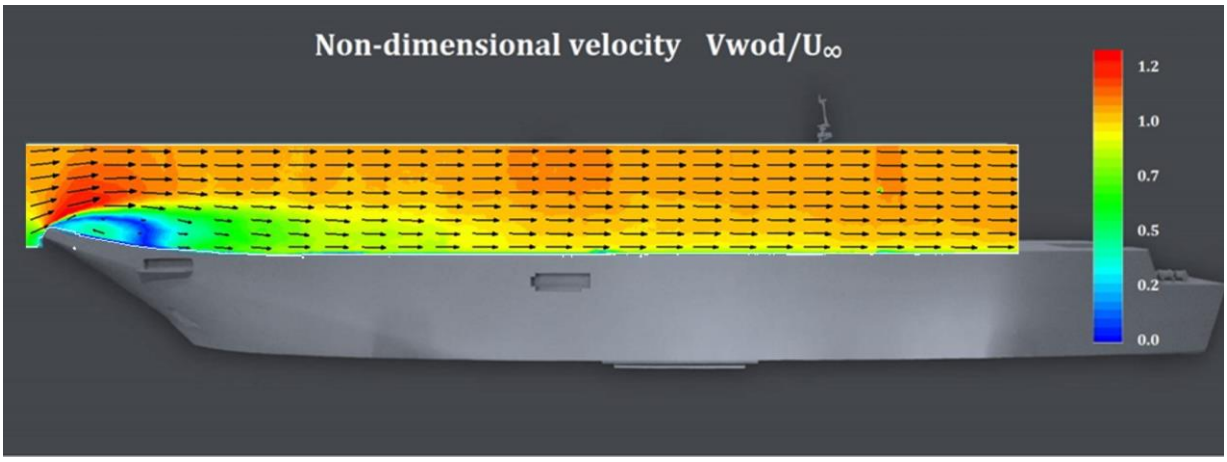

Figure 7. Non-dimensional velocity obtained by PIV.

Figure 8 shows a more detailed view of the flow velocity over the ski-jump ramp. Streamlines are overlapped over the velocity map indicating the flow direction. The map shows a region of low velocity, corresponding with the structure of a recirculation bubble. The size of the bubble, defined by h_b can be measured as the maximum distance from the surface of the ramp to the top of the bubble, and it is of the order of the height of the ramp itself ($h_b/h \sim 1$). Strong velocity gradients appear inside the recirculation region. The highest flow velocity corresponds to a value of 1.3 U_∞ located in the boundaries of the bubble. It has also been indicated in the figure the reattachment point and the aircraft wing path. The reattachment point is located at $\hat{x} = 0.9$, which is the 90% of the take-off distance. From that point on the air flow direction is reversed up to the point when the aircraft leaves the recirculation bubble, which

Published by the American Institute of Aeronautics and Astronautics, Inc., with permission. Complete Citation: Bardera-Mora, R., Garcia-Magariño, A., Rodríguez-Sevillano, A., & Barcala-Montejano, M. A. (2019). Aerodynamic flow effects on aircraft carrier takeoff performance. Journal of Aircraft, 56(3), 1005-1013. https://doi.org/10.2514/1.C035188

happens at 99% of the take-off distance. The reattachment point is also observed in Fig. 4. The implications of the recirculation bubble in the take-off manoeuvre is studied in the following sections.

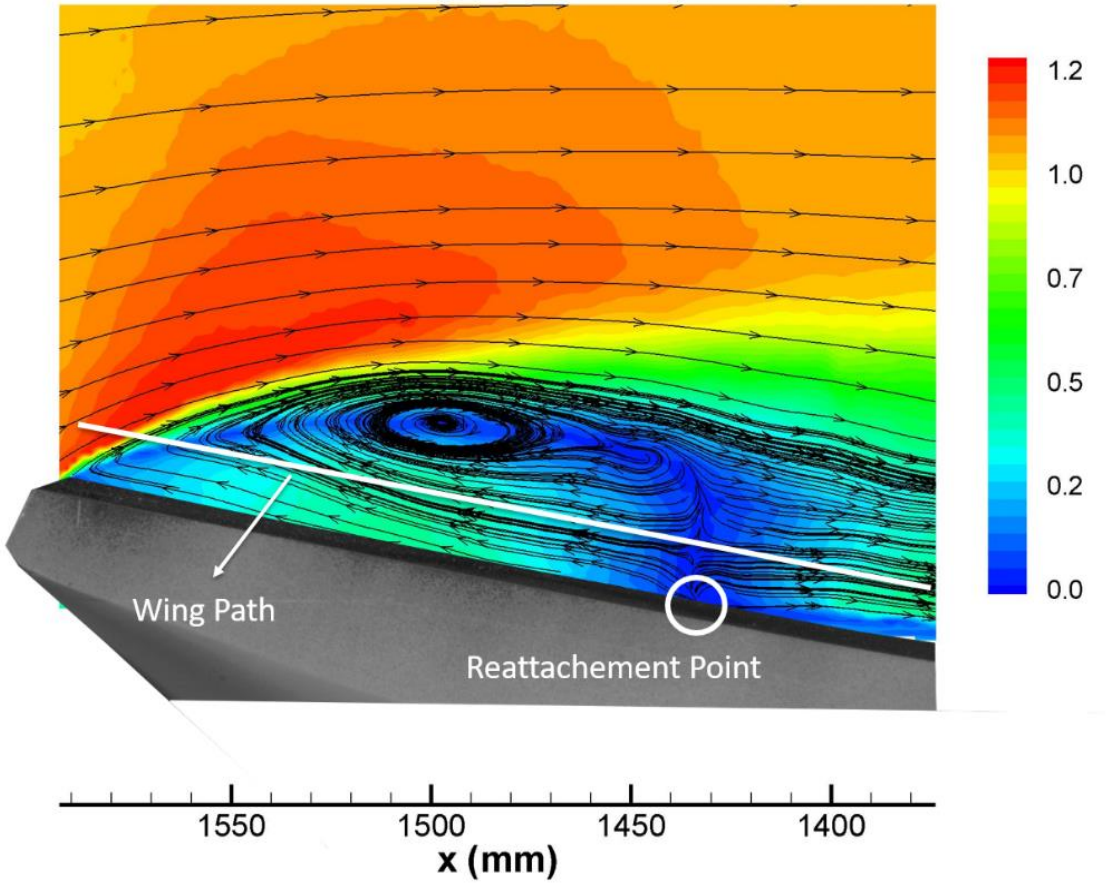

Figure 8. Non-dimensional velocity field over take-off ramp.

Figure 9 shows the turbulence intensity (TI) above the flight deck of the aircraft carrier defined as follows:

$$\mathrm{TI}\ (\%) = 100 \cdot \frac{\sigma_{\mathrm{tot}}}{\mathrm{U}_{\infty}} \tag{22}$$

where a reference mean velocity (the freestream velocity U_{∞}) and the total standard deviation have been used. The square of the total standard deviation σ_{tot} is calculated as the sum of the standard deviation of the horizontal and

Published by the American Institute of Aeronautics and Astronautics, Inc., with permission. Complete Citation: Bardera-Mora, R., Garcia-Magariño, A., Rodríguez-Sevillano, A., & Barcala-Montejano, M. A. (2019). Aerodynamic flow effects on aircraft carrier takeoff performance. Journal of Aircraft, 56(3), 1005-1013. https://doi.org/10.2514/1.C035188

vertical components of the velocity. This map (Fig. 9) shows high values in the region bounding the bubble, forming a shear layer.

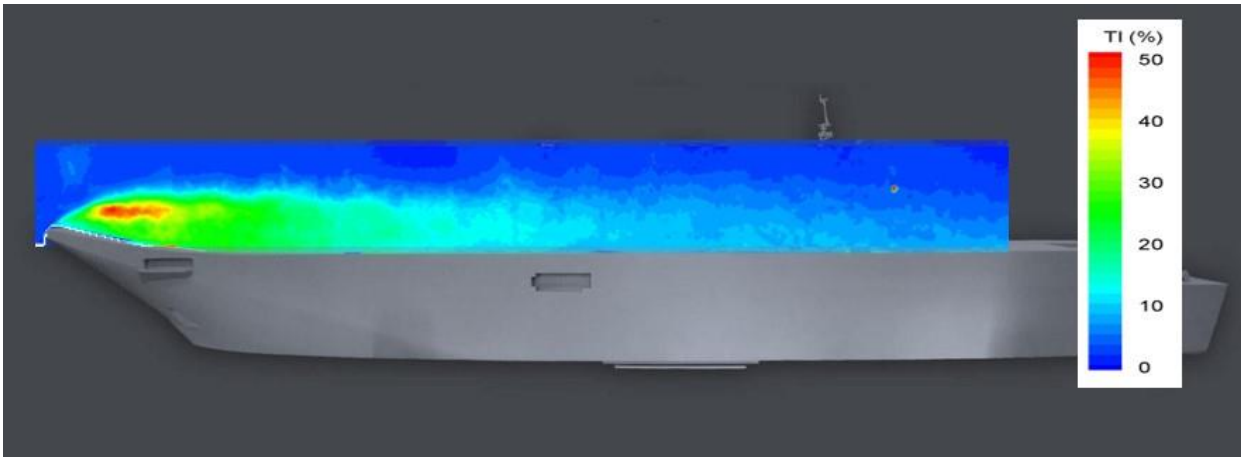

Figure 9. Turbulence Intensity all over the flow deck.

Figure 10 shows turbulence intensity in frame 1 over the take-off ramp. A turbulent shear layer appears around the recirculation bubble, showing large fluctuating values of the stream velocity. Maximum turbulence intensity appears in the turbulent shear layer with values of the order of 50%.

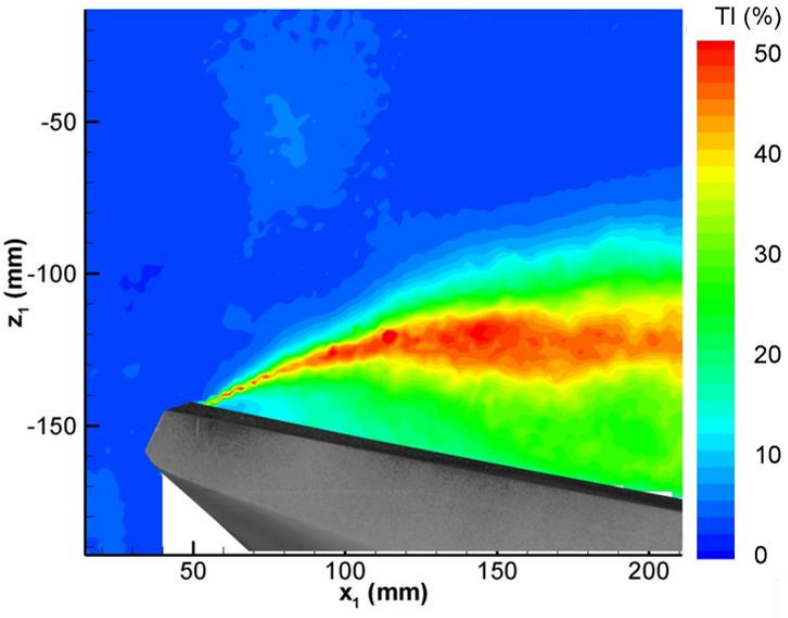

Figure 10.Intensity turbulence in frame 1 over take-off ramp.

Published by the American Institute of Aeronautics and Astronautics, Inc., with permission. Complete Citation: Bardera-Mora, R., Garcia-Magariño, A., Rodríguez-Sevillano, A., & Barcala-Montejano, M. A. (2019). Aerodynamic flow effects on aircraft carrier takeoff performance. Journal of Aircraft, 56(3), 1005-1013. https://doi.org/10.2514/1.C035188

High levels of turbulence has strong effect on the aerodynamic forces (lift and drag), since turbulence intensity represents the velocity fluctuations and aerodynamic forces are proportional to the square of the velocity ($L \propto V^2 \; and \; D \propto V^2$). Consequently, high fluctuations in lift and drag will be expected in high turbulence regions.

IV. AV-8B Harrier's short take-off performance

The effects of the aerodynamic disturbances caused by the ski- jump ramp are evaluated in this section. A practical application is included in order to quantify these effects. First, the take-off manoeuvre of the AV-8B Harrier II in a ski-jump ramp flight deck is analysed. This aircraft has been selected because of its frequent operation in this kind of aircraft carrier. Then, the performance will be compared with those of the same aircraft taking-off in a flat deck of the same horizontal length.

A. Take-off performance over Ski Jump Ramp

As it has been explained before in section 2, the study of take-off Flight Mechanics for a ski-jump flight deck led to the Eq. (15) for the horizontal part (0-1) and (16) for the curved part of the deck (1-2). It can be seen in both equations that the wind over deck velocity is needed along the aircraft's wing path in order to calculate the aerodynamic velocity. Wind tunnel tests have been carried out in order to determine this velocity along the take-off runway. The aircraft's wing path is represented in red color in Fig. 11. Based on the height at the root and at the tip, an average wing height has been calculated, resulting in a value of 1.5 m at full scale.

Published by the American Institute of Aeronautics and Astronautics, Inc., with permission. Complete Citation: Bardera-Mora, R., Garcia-Magariño, A., Rodríguez-Sevillano, A., & Barcala-Montejano, M. A. (2019). Aerodynamic flow effects on aircraft carrier takeoff performance. Journal of Aircraft, 56(3), 1005-1013. https://doi.org/10.2514/1.C035188

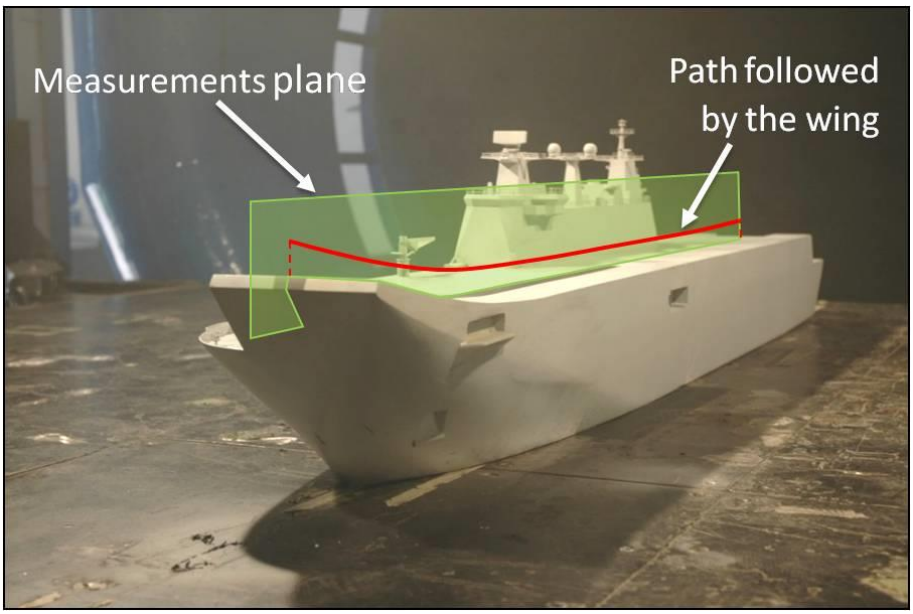

Figure 11.Trajectory described by the wing along the take-off run.

PIV measurements have been taken along a plane perpendicular to the flight deck that passes through the middle of the take-off runway as explained in previous section (see again Fig. 11). Both, parallel $\hat{V}_{WOD_{\parallel}}$ and perpendicular $\hat{V}_{WOD_{\perp}}$ wing over deck dimensionless velocity components have been obtained along the path followed by the wing. Fig. 12 shows a plot of these velocities components against the dimensionless horizontal position $\hat{x} = x/Lto$.

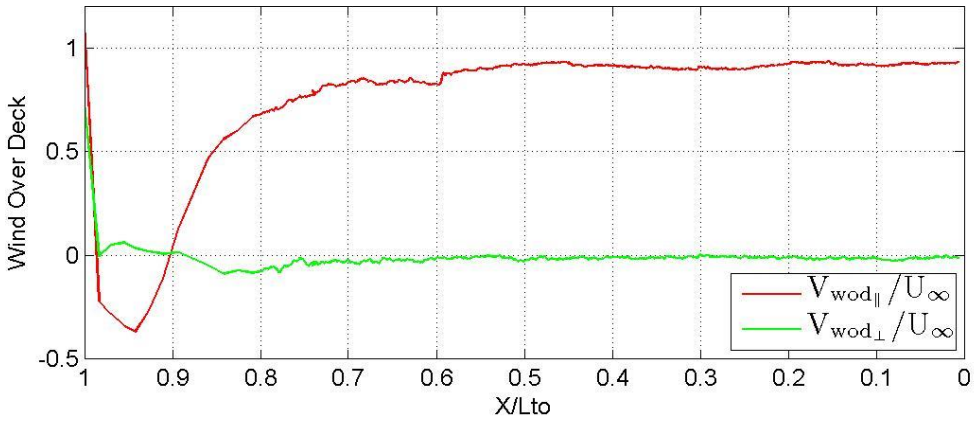

Figure 12. Representation of both parallel and perpendicular components of the Wind Over Deck (U_{∞} is the undisturbed fluid velocity).

Published by the American Institute of Aeronautics and Astronautics, Inc., with permission. Complete Citation: Bardera-Mora, R., Garcia-Magariño, A., Rodríguez-Sevillano, A., & Barcala-Montejano, M. A. (2019). Aerodynamic flow effects on aircraft carrier takeoff performance. Journal of Aircraft, 56(3), 1005-1013. https://doi.org/10.2514/1.C035188

As observed in Fig. 12, during the first 60% of the take-off run the flow velocity is nearly parallel to the deck and thus, the contribution of the normal component is very small. In this first part of the take-off run, the parallel component is around 10% below the undisturbed velocity U_∞.

The second part, the rest 40% of the take-off run, is characterised by a sharp decrease of the parallel velocity as the aircraft enters the recirculation bubble. This is a region of separated flow where the velocity of the wind over deck is very low and the parallel velocity component has even the opposite direction. Then, after reaching a value of

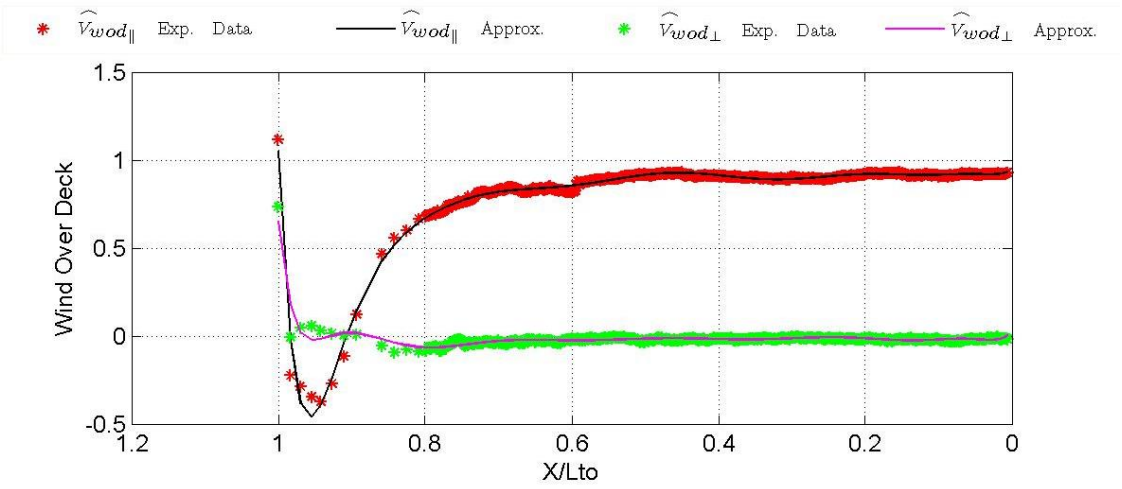

Figure 13. Fitting of both parallel and perpendicular components of the Wind Over Deck.

$\widehat{V}_{WOD_\parallel} = -0.4$, both components grow abruptly because of the aircraft's exit from the bubble.

To analyse the take-off performance of this aircraft, it was decided to obtain the analytical function of the wind over deck velocity components along the wing path in order to facilitate the numerical resolution of the equations. The experimental results have been approximated by a polynomial interpolation of degree 12, obtaining the following analytical functions:

$$\widehat{V}_{WOD_\parallel}(\hat{x}) = a_0 + \sum_{i=1}^{12} a_i \hat{x}^i \tag{23}$$

$$\widehat{V}_{WOD_\perp}(\hat{x}) = b_0 + \sum_{i=1}^{12} b_i \hat{x}^i \tag{24}$$

Published by the American Institute of Aeronautics and Astronautics, Inc., with permission. Complete Citation: Bardera-Mora, R., Garcia-Magariño, A., Rodríguez-Sevillano, A., & Barcala-Montejano, M. A. (2019). Aerodynamic flow effects on aircraft carrier takeoff performance. Journal of Aircraft, 56(3), 1005-1013. https://doi.org/10.2514/1.C035188

where a_i and b_i are the approximation coefficients (see table 1) and $\hat{x}$ is the non-dimensional coordinate along the take-off run defined as the local take-off spatial coordinate x divided by the total take-off distance Lto ($\hat{x} = 0$ at the starting point and $\hat{x} = 1$ at the end of the ramp). The polynomial fitting is represented in Fig. 13.

Table 1. Approximation coefficients.

i	a_i	b_i
0	9.515E-01	3.039E-02
1	-2.965E+00	-4.775E+00
2	1.119E+02	1.687E+02
3	-2.084E+03	-2.857E+03
4	2.168E+04	2.695E+04
5	-1.363E+05	-1.552E+05
6	5.455E+05	5.769E+05
7	-1.431E+06	-1.426E+06
8	2.492E+06	2.367E+06
9	-2.850E+06	-2.606E+06
10	2.059E+06	1.825E+06
11	-8.515E+05	-7.349E+05
12	1.537E+05	1.296E+05

In order to solve the equations of motion of the aircraft during the take-off operation, the following parameter values are assumed, weight W = 138321 N, wing area S = 22.61 m^2, maximum thrust Tmax = 104500 N, gravity g = 9.81 m/s^2, air density ρ = 1.225 kg/m^3, radius of curvature of the ramp R = 165 m and take-off distance Lto = 216 m.

In addition, some typical values have been chosen for the remaining parameters[25] as medium wind intensity over the sea surface V_W = 10 m/s, carrier's velocity V_S = 10 m/s, and coefficient of rolling friction μ = 0.02. For the aerodynamic coefficients, a typical value for take-off configuration has been chosen[26]: $C_{L0} = 1.465$, $C_{L_\alpha} = 2\pi$, $C_{D0} = 0.064$, and $k = 0.060$.

The relation between the non-dimensional take-off run length parameter $\hat{x}$ and the local angle of circular arc θ is included:

$$\hat{x} = \hat{x}_1 + \frac{R}{L_{to}} \sin\theta \tag{25}$$

where $\hat{x}_1 = 0.8412$ is the value of $\hat{x}$ at the end of the flat part.

Thus, it is possible to solve the Eqs. (15) and (16) in order to obtain the velocity of the aircraft relative to the carrier $\hat{V}_f$ as a function of the longitudinal dimensionless position $\hat{x}$. The resolution of these differential equations has been carried out numerically by using a Runge-Kutta 4.5 method implemented in an in-house developed Matlab code. Once V_f is obtained, the aerodynamic velocity V_a can be calculated as follows:

Published by the American Institute of Aeronautics and Astronautics, Inc., with permission. Complete Citation: Bardera-Mora, R., Garcia-Magariño, A., Rodríguez-Sevillano, A., & Barcala-Montejano, M. A. (2019). Aerodynamic flow effects on aircraft carrier takeoff performance. Journal of Aircraft, 56(3), 1005-1013. https://doi.org/10.2514/1.C035188

$$V_a^{\,2} = (V_{wod\_\parallel} + V_f)^2 + V_{wod\_\perp}^{\,2} \tag{26}$$

In Fig. 14, the aerodynamic velocity along the take-off run against the dimensionless horizontal position is represented. The first part of the curve corresponds to the flat region and the second one to the curved region.

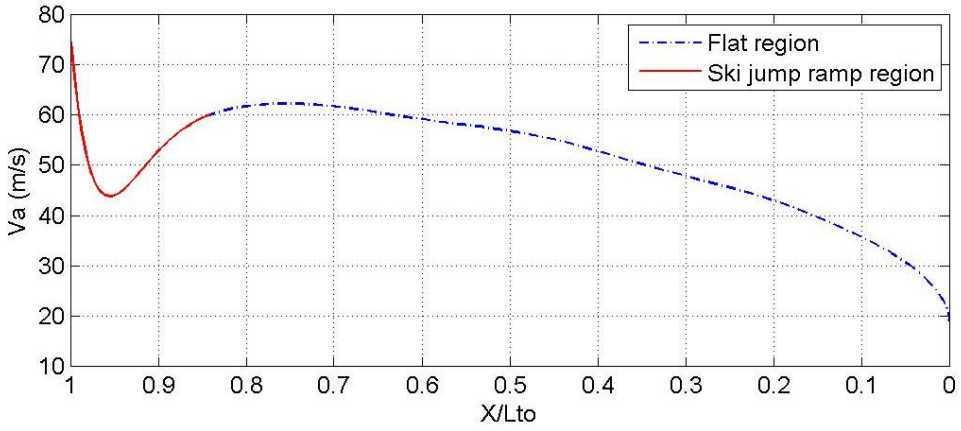

Figure 14. Aerodynamic velocity V_a along the take-off run with VWOD = 20 m/s.

It is apparent in Fig. 14 the decrease of the aerodynamic velocity inside the recirculation bubble at the ramp. A possible way to reduce this aerodynamic velocity drop-out in the ski-jump ramp would be an active flow control based on blowing the boundary layer where the recirculated bubble is installed above the ski-jump ramp. Further studies could be done in this direction. On the other hand, the velocity grows sharply as the aircraft leaves the bubble, with the aerodynamic velocity at the end of the take-off run being 74.52 m/s (268.27 km/h). The decrease in the aerodynamic velocity will lead to a decrease in the lift and the drag forces as observed in Fig. 15, where both forces are plotted. The lift and drag along the take-off run are calculated using the Eqs.(2-5) and Eq. (9).

Published by the American Institute of Aeronautics and Astronautics, Inc., with permission. Complete Citation: Bardera-Mora, R., Garcia-Magariño, A., Rodríguez-Sevillano, A., & Barcala-Montejano, M. A. (2019). Aerodynamic flow effects on aircraft carrier takeoff performance. Journal of Aircraft, 56(3), 1005-1013. https://doi.org/10.2514/1.C035188

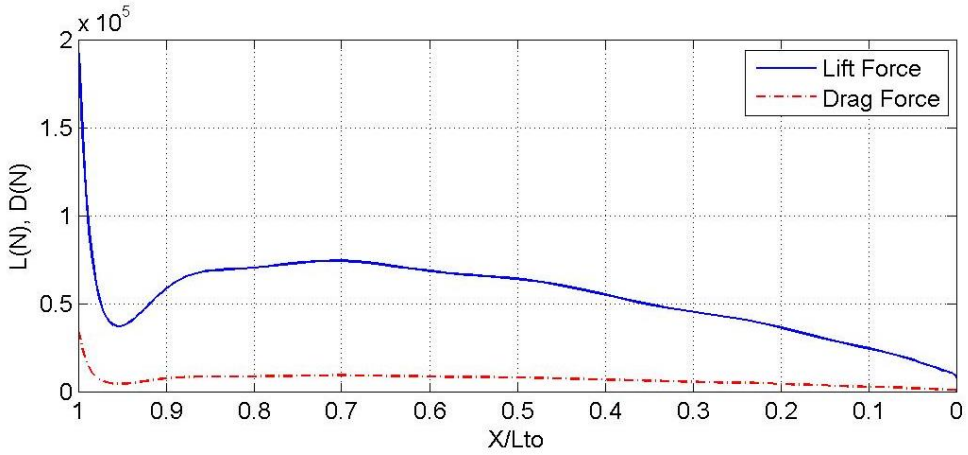

Figure 15. Lift (L) and drag (D) forces along the take-off run.

On the one hand, there is a reduction of the aerodynamic drag that would allow the aircraft to accelerate more, however, on the other hand, the reduction in lift increases the friction force, which prevents the aircraft to accelerate more. It is interesting to see the magnitude of all the forces during the take-off. This has been done in Fig. 16. It can be observed that the friction force is, in general, smaller than the drag force, which is predominantly the effect of the reduction in the drag coefficient.

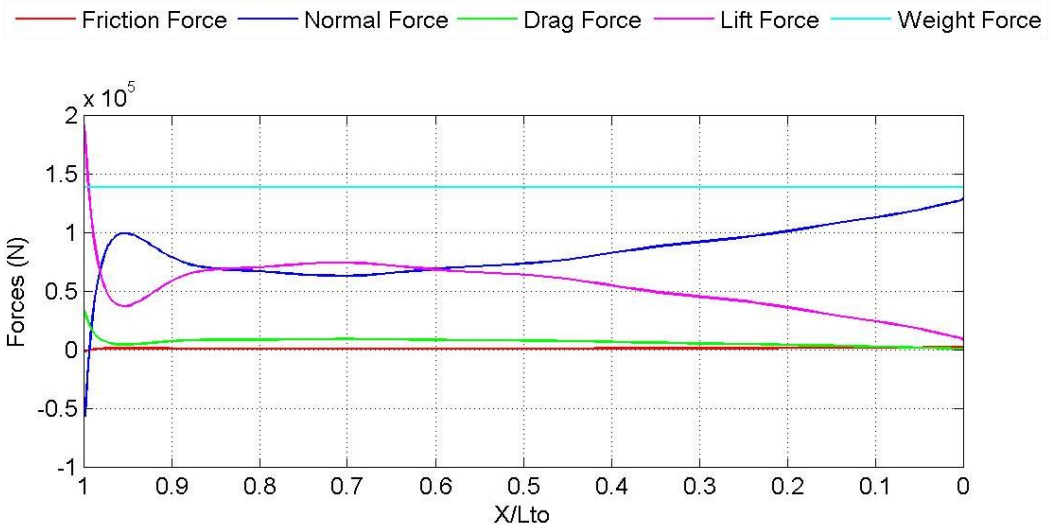

Figure 16. Forces on the aircraft along the take-off run.

Published by the American Institute of Aeronautics and Astronautics, Inc., with permission. Complete Citation: Bardera-Mora, R., Garcia-Magariño, A., Rodríguez-Sevillano, A., & Barcala-Montejano, M. A. (2019). Aerodynamic flow effects on aircraft carrier takeoff performance. Journal of Aircraft, 56(3), 1005-1013. https://doi.org/10.2514/1.C035188

Finally, it is also interesting to observe that the sharp increment in the lift as the aircraft leaves the recirculation bubble can induce large load factors affecting the aircraft structure. This has to be studied and to this end the load factor defined as $n = L/W$ is plotted in Fig. 17. It is observed that there is a change in the load factor of 1.4 at the exit of the bubble.

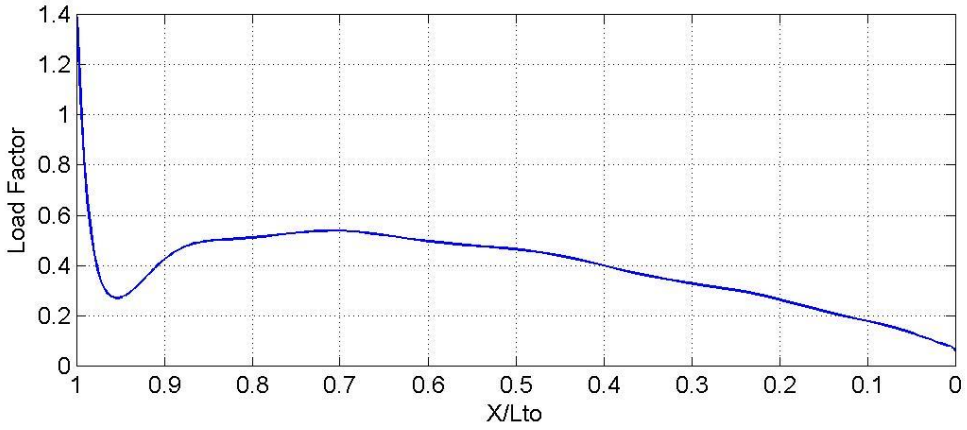

Figure 17. Load factor along the take-off run.

B. Comparison between flat deck and Ski Jump Ramp performance

In this section the take-off performance using ski-jump ramp analyzed in the previous section is compared to the performance of the same aircraft taking off from an entirely flat deck of the same length (Lto = 216 m). The objective is to determine the aerodynamic advantages and disadvantages of one with respect to the other. The same take-off conditions are applied for both cases, in particular $U_\infty = V_W + V_S = 20\ m/s$. In the case of entirely flat deck, the assumption of uniform velocity parallel to the deck is made, $\vec{V}_{WOD_{flat\ deck}} = -U_\infty \vec{u}_\parallel$. Equation (15) is solved for this case considering that $\widehat{V}_a = 1 + \widehat{V}_f$ and $\alpha = 0$ all along the take-off.

In Figs. 18 and 19 the aircraft and aerodynamic velocities are compared for both cases. The dashed red curve represents the operation using the ski jump ramp and the continuous blue curve describes the performance over an entirely flat deck. It can be observed in Fig. 18 that the final aircraft velocity at the end of the ramp is similar for both cases. For the case of the ski-jump ramp, the aircraft not only moves horizontal but it also goes up, thus increasing its potential energy. On the other hand, as discussed in previous section, the decrease in the air velocity during the

Published by the American Institute of Aeronautics and Astronautics, Inc., with permission. Complete Citation: Bardera-Mora, R., Garcia-Magariño, A., Rodríguez-Sevillano, A., & Barcala-Montejano, M. A. (2019). Aerodynamic flow effects on aircraft carrier takeoff performance. Journal of Aircraft, 56(3), 1005-1013. https://doi.org/10.2514/1.C035188

recirculated region aided the aircraft to accelerate more. In the end, the dissipation energy saved due to the decreased in the aerodynamic drag during the recirculated region is counteracted by the increase in the potential energy and the final aircraft velocity is similar for both cases (flat deck and ski-jump ramp deck).

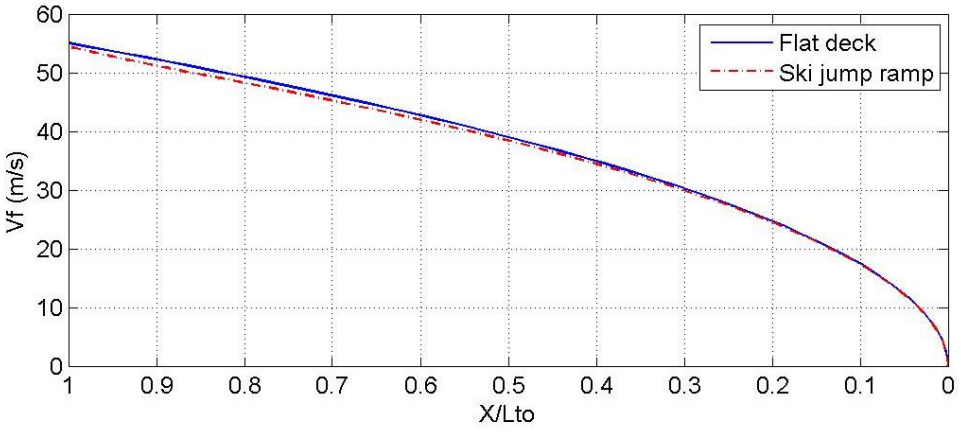

Figure 18. Aircraft velocity V_f comparison between the operations carried out over flat deck and Ski Jump Ramp.

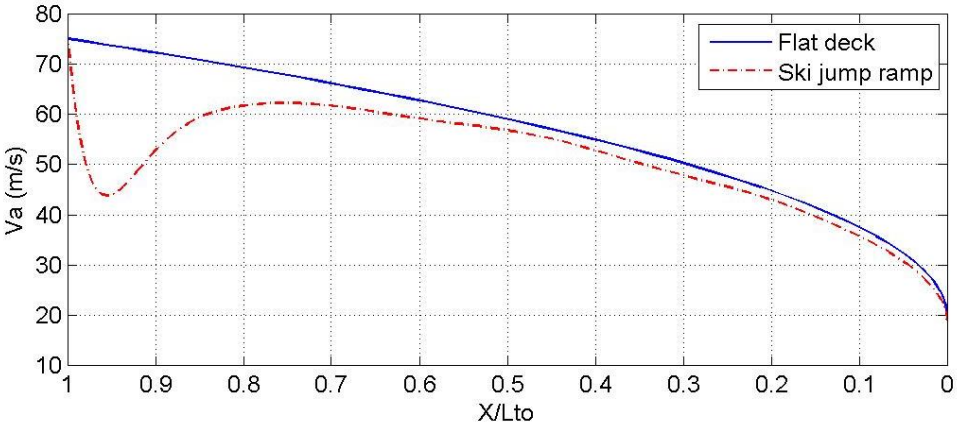

Figure 19. Aerodynamic velocity V_a comparison between the operations carried out over flat deck and Ski-Jump Ramp.

One of the effects of the ski-jump ramp over the rest of the deck is that it reduces the velocity of the wind over deck. This results in a decrease of the aerodynamic velocity with respect to the flat deck case and this is why the

Published by the American Institute of Aeronautics and Astronautics, Inc., with permission. Complete Citation: Bardera-Mora, R., Garcia-Magariño, A., Rodríguez-Sevillano, A., & Barcala-Montejano, M. A. (2019). Aerodynamic flow effects on aircraft carrier takeoff performance. Journal of Aircraft, 56(3), 1005-1013. https://doi.org/10.2514/1.C035188

dashed red curve always remains below the blue one in Fig. 19. However, the increment of wind over deck velocity that occurs when the aircraft exits the bubble leaves the aerodynamic velocity only 0.9 m/s below the velocity in the flat deck case.

If the lift forces for both cases are calculated based on the velocity curves from Fig. 19, the following graph can be obtained.

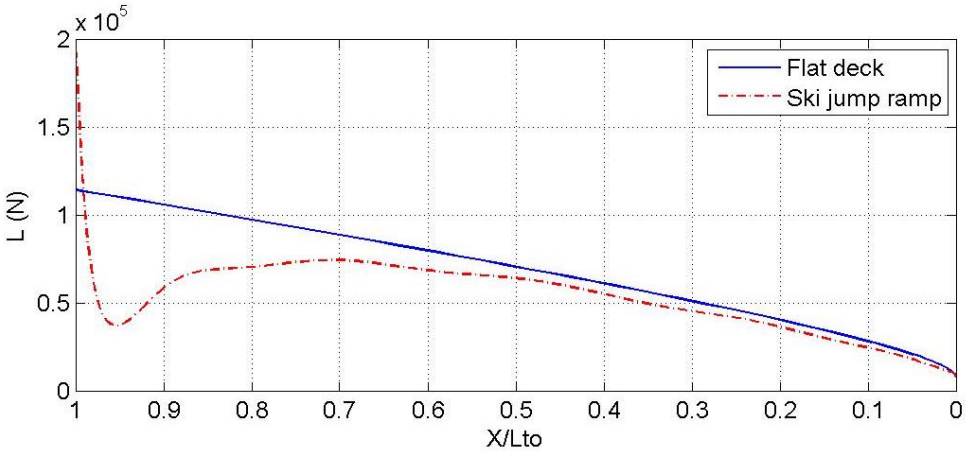

Figure 20. Lift (L) comparison between flat deck and ski-jump ramp operations.

It can be observed in Fig. 20 that the lift force is, in general, smaller for the ski-jump deck except at the end of the ramp. The lift force value at the end of the ramp for each case is included below:

$$L_{\text{flat deck}} = 1.166 \times 10^5 \text{ N} \quad (27)$$

$$L_{\text{ski jump ramp}} = 1.922 \times 10^5 \text{ N} \quad (28)$$

Published by the American Institute of Aeronautics and Astronautics, Inc., with permission. Complete Citation: Bardera-Mora, R., Garcia-Magariño, A., Rodríguez-Sevillano, A., & Barcala-Montejano, M. A. (2019). Aerodynamic flow effects on aircraft carrier takeoff performance. Journal of Aircraft, 56(3), 1005-1013. https://doi.org/10.2514/1.C035188

The spectacular increase of the lift of 65% at the end of the ski-jump ramp that the aircraft experiences is due to two reasons. Firstly, the aircraft leaves the recirculation bubble and the aerodynamic velocity increases. Secondly, there is a high increase in the angle of attack. To understand this fact, Fig. 21 shows a sketch of what happens. During the take-off runway the wind over deck is almost parallel to the deck, except in the recirculation region. However, when the aircraft leaves the ship, at the end of the ramp, the velocity becomes horizontal, thus inducing an increase in the angle of attack.

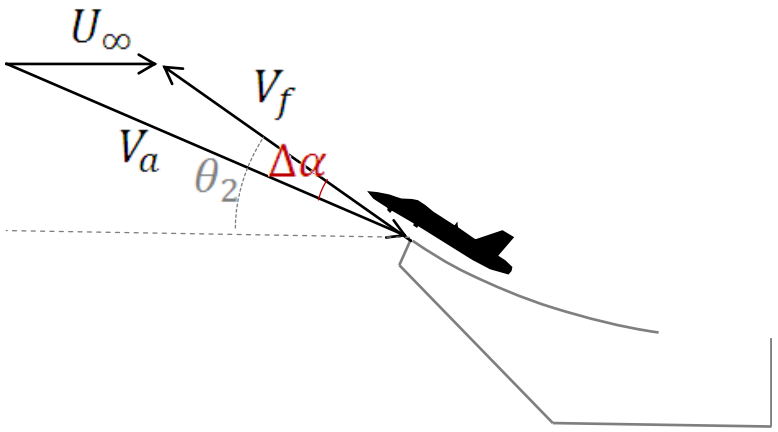

Figure 21. Velocity diagram at the time the aircraft leaves the ramp.

V. Summary & Conclusions

The ski-jump ramp is a very advantageous device in maritime aircraft operations on board aircraft carriers, allowing the airplane to gain extra lift in adverse operational conditions but it is built based on sharp-edged geometries that produce aerodynamic disturbances on the flow field present in the flight deck, affecting the aircraft manoeuvres.

The flow field above the ski-jump deck of an aircraft carrier was investigated using wind tunnel testing a sub-scale model, in order to get a more precise insight about the flow developed over this region of the ship.

Firstly, smoke visualizations were performed over the flight deck of the ship. The visualization showed turbulent nature of the flow and the formation of a recirculation bubble over the ramp with strong vortex shedding throughout the flight deck.

Particle Image Velocimetry (PIV) was used to characterize the flow field velocity over the flight deck. PIV results have been presented by classical maps. The velocity map of the flow over the ski-jump ramp showed a recirculation region whose size was of the order of the height of the ramp itself. Strong velocity gradients appeared inside the bubble

Published by the American Institute of Aeronautics and Astronautics, Inc., with permission. Complete Citation: Bardera-Mora, R., Garcia-Magariño, A., Rodríguez-Sevillano, A., & Barcala-Montejano, M. A. (2019). Aerodynamic flow effects on aircraft carrier takeoff performance. Journal of Aircraft, 56(3), 1005-1013. https://doi.org/10.2514/1.C035188

with approximate wind velocity values from $-0.4U_\infty$ to $1.3U_\infty$. The turbulence map showed the turbulence intensity distribution over the ramp indicating maximum turbulence level of 50% of the freestream velocity in the turbulent shear layer that surrounds the bubble. More efforts could be done in the future to study the implications of these aerodynamic aspects.

After analysing the flow over the deck, the influence of this particular flow in the take-off performance of an AV-8B Harrier II was evaluated. The main conclusions can be stated:

- The research revealed that the aerodynamic disturbances caused by the ramp lead to similar aerodynamic velocity at the end of the ramp compared with a flat deck. However, there is an increase in the lift at the end of the ramp as high as 65% due to the increase in the angle of attack.
- The aircraft velocity at the end of the ramp is similar compared with that in a flat deck although there is an increase in the potential energy of the aircraft. This is due to the appearance of recirculated region and consequently the decrease in the aerodynamic drag.
- At the end of the recirculation bubble the load factor changes sharply in a very short time. This could induce structural problems that have to be taken into account.

Finally, we can conclude that this study provided a detailed characterization of the flow over the ski-jump take-off runway and the aerodynamic advantages and disadvantages that it provides, resulting in a useful research for future studies on aircraft-ship interference directed to reduce the risk in aircraft carrier operations.

Acknowledgments

This investigation was funded by Spanish Ministry of Defense under the INTA program “Termofluidodinámica”.

References

[1]Liu, D., Liu, G., and Hong, G. “Analysis of on board take-off and landing characteristics for unmanned aerial vehicles”, *AIAA Modelling and Simulation Technologies Conference*, 2016.

[2]Ryan J. C., and Cummings M. L. “A systems analysis of the introduction of unmanned aircraft into aircraft carrier operations”, *IEEE Transactions on human-machine systems*, 46 (2), 2016.

[3]Lumsden, R. B. Ship Air-Wake Measurement, Prediction, Modelling and Mitigation. Air Vehicle Concepts and Performance, 2003.

[4]Doyle M. R., Samuel D. J., Conway T. and Klimowski R. R., "Electromagnetic aircraft launch system –EMALS", *IEEE Transactions on magnetic*, 31 (1), 1995.

[5]Weijun W., Xiangju Q. and Linliang G., "Multi-agent based hierarchy simulations models of carrier-based aircraft catapult launch", *Chinese Journal of Aeronautics* 21 (2008) 223-231.

[6]CTOL ski jump - Analysis, simulation, and flight test J. W. CLARK, M. WALTERS Journal of Aircraft, 1986, Vol.23: 382-389, 10.2514/3.45319

[7]Method for analyzing the influence of random factors in carrier launching Zhu Qian, Wang Weijun, Qu Xiangju AIAA Atmospheric Flight Mechanics Conference, 2012, 10.2514/6.2012-4643

[8]Bardera-Mora R., Barcala-Montejano M. A., Rodríguez-Sevillano A., Nova-Trigueros J., "Passive flow control over the ski-jump of aircraft carriers", *Ocean Engineering*, 114 (2016) pp. 134-141. Elsevier, Ltd.

[9]Fozard, J. W., "Ski-jump – A great leap for tactical airpower", *British aerospace paper* 79-0696, 1979.

[10]Fry A., "CVF ski-jump ramp profile optimization for F-35B", *The Aeronautical Journal*, 113 (1140) 79-85, 2009

[11]Wei-Wei L. and Xiang-Ju Q., "Modeling of carrier-based aircraft ski-jump take-off based on tensor". *Chinese Journal of Aeronautics* 18 (4) 326-335, 2005.

[12]Yangang W., Weijun, W. and Xianju, Q., "Multi-body dynamic system simulation of carrier-based aircraft ski-jump take-off". *Chinese Journal of Aeronautics* 26 (1) 104-111, 2013.

[13]Hernando, J.L.,Martínez-Val, R. "Carrier Suitability of Land-Based Aircraft". *ICAS2012, 28th International Congress of the Aeronautical Sciences*, 2012.

[14]Miele, A. Flight Mechanics Volume 1: Theory of Flight Paths. 1st Ed.; Addison-Wesley Pub. 1962.

[15]Barlow, J. B., Rae, W. H. Jr.; Pope, "A. Low-Speed Wind Tunnel Testing". *3rd Ed.; John Wiley & Sons, Inc.* USA 1999.

[16]Anderson, J. D., "Aircraft Performance and Design". McGraw-Hill Companies, Inc. 1999.

[17]Healey, J. V. "Establishing database for flight in the wake of structures". *Journal of Aircraft* 1992, Vol. 29, No. 4, pp. 559-564.

[18]Raffel, M.,Willert, C. E.,Wereley, S. T.; Kompenhans, J. "Particle Image Velocimetry: A Practical Guide". Springer, 2007.

[19]Kompenhans, J.,Raffel, M.,Willert, M. "PIV Applied to Aerodynamic Investigations in Wind Tunnels". *Von Karman Institute for Fluid Dynamics* 1996, Lectures Series 1996-03, Rhode Saint Genese, Belgium.

Published by the American Institute of Aeronautics and Astronautics, Inc., with permission. Complete Citation: Bardera-Mora, R., Garcia-Magariño, A., Rodríguez-Sevillano, A., & Barcala-Montejano, M. A. (2019). Aerodynamic flow effects on aircraft carrier takeoff performance. Journal of Aircraft, 56(3), 1005-1013. https://doi.org/10.2514/1.C035188

[20]Adrian, R. J.,Westerweel, J. “Particle Image Velocimetry”, *Cambridge University Press*, 2011.

[19]Adrian, R. J. “Particle-imaging techniques for experimental fluid mechanics”. *Annual Review of Fluid Mechanics* 1991, 23: 261-304.

[20]Echols, W. H.,Young, Y. “A. Studies of portable air-operated aerosol generator”. NRL Report 5929, Naval Research Laboratory, Washington, D. C., 1963.

[21]Kähler, C. J.,Sammler, B.,Kompenhans, J. “Generation and control of tracer particles for optical flow investigation in air”. *Experiments in Fluids* 2002, 33, 736-742.

[22]Prasad, A. K. “Particle Image Velocimetry”. Current Science, Vol. 79, no. 1, 10, 2000.

[23]Hull, D. G. “Fundamentals of Airplane Flight Mechanics”. Springer-Verlag Berlin Heidelberg, 2007.

[24]McNally, B. David. “Full-envelope aerodynamic modeling of the Harrier Aircraft”.1986.